LA-6069-MS

c.3

UC-25
Reporting Date: August 1975
Issued: December 1975

High-Density Metals and Metallic Composites for Improved Fragmentation Submunitions

by

B. G. Craig
R. E. Honnell
G. F. Lederman, Jr.
D. J. Sandstrom

los alamos
scientific laboratory
of the University of California
LOS ALAMOS, NEW MEXICO 87545

An Affirmative Action/Equal Opportunity Employer

UNITED STATES
ENERGY RESEARCH AND DEVELOPMENT ADMINISTRATION
CONTRACT W-7405-ENG. 36

This work was supported by the U.S. Army Materiel Systems Analysis Activity (AMSAA).

Printed in the United States of America. Available from
National Technical Information Service
U.S. Department of Commerce
5285 Port Royal Road
Springfield, VA 22151
Price: Printed Copy $5.00 Microfiche $2.25

HIGH-DENSITY METALS AND METALLIC COMPOSITES FOR IMPROVED FRAGMENTATION SUBMUNITIONS

by

B. G. Craig, R. E. Honnell,
G. F. Lederman, Jr., and D. J. Sandstrom

ABSTRACT

The fragmentation of cases (50.8-mm-i.d.) made of tungsten, a tungsten alloy, and depleted uranium (D-38) can be controlled, and velocities >1 mm/μs can be achieved for lethal size fragment weights. Fragmentation was controlled by internal grooves, by internal screens, and by a spheroid-in-weak-matrix scheme. A thin polymer liner was used inside of a grooved tungsten case in one experiment; this system performed exceptionally well. The ease of fabricating cases with D-38 or with the tungsten-alloy spheroid-in-matrix scheme offers an attractive advantage over tungsten and tungsten alloy.

I. INTRODUCTION

Replacement of steel by high-density metals in fragmenting submunitions would enhance their lethality provided that other lethality parameters were not adversely affected to a significant degree by the substitution. It requires more than five times the thickness of armor to stop a 0.5-g spherical tungsten fragment than is required to stop a 1-g spherical steel fragment at the same given velocity.

A practical heavy-metal submunition is one that can be mass produced at reasonable material cost. The cost of material eliminates such candidates as tantalum, rhenium, and the precious metals; hence the best candidates are depleted uranium (D-38), tungsten, and tungsten alloys. Depleted uranium is attractive because it can be cold worked, is in abundant supply, and costs $1/kg (one-twelfth the cost of tungsten). Moreover, D-38 fragments are pyrophoric which makes them more effective against particular targets. Its potential drawbacks are limited shelf life, unless protected from excessive oxidation, and the environmental and political repercussions of releasing such fragments into the biosphere. Although tungsten avoids these liabilities, it does not lend itself to mechanical working processes. Tungsten is usually fabricated into intricate shapes by powder metallurgical techniques. Machining is generally limited to grinding and electrical discharge machining. However, the workability and machinability of tungsten can be improved by alloying it with small amounts of iron, nickel, and/or copper.

A study was undertaken at the Los Alamos Scientific Laboratory (LASL) for the Army Materiel Systems Analysis Activity (AMSAA) to demonstrate the feasibility of fabricating heavy-metal controlled-fragmentation submunitions. Performance goals were twofold: (1) that the device fragment into about 0.45-g (7-grain) pieces with peak velocities of at least 1.0 mm/μs and (2) that the munition fabrication process lend itself to mass production. The outer dimensions of the heavy-metal munitions were to approximate those of the Bomb Line Unit, BLU-63 (~53-mm o.d.), a scored-steel antipersonnel submunition presently in field use.

The scope of the study was to fabricate, characterize, and ballistically test five configurations of D-38, tungsten, and tungsten alloy, and make one proof shot of the most promising system. Brief descriptions follow of the heavy-metal

cases (Sec. II), explosive system (Sec. III), experimental technique (Sec. IV), and ballistic results (Sec. V).

One-dimensional hydrodynamic calculations were performed to provide guidance for selecting an explosive fill and for selecting case thickness and material(s) that would have a potential for achieving the desired fragment velocity. Pertinent calculations are presented in Sec. VI. Further fabrication details of the heavy-metal cases are given in Sec. VII.

II. HEAVY-METAL CASES

Case data for six test firings are compiled in Table I. Test 6 was a duplication of Test 3. Several of the configurations used different materials for each of the hemispheres; in some instances each quadrant of a configuration was prepared for firing in a slightly different way. In this way, 15 case configurations were examined in the 6 test firings. Figure 1 shows a typical assembly procedure (see p. 14).

TABLE I

HEAVY-METAL CASE DATA

Test No. (Shot No.)	Hemishell Configuration	Mass (g)	Density (g/cm^3)	Designed Fragment Weight and Yield (g)	(grains)	(No./Hemishell)	Outside Diameter (mm)	Wall Thickness (mm)	Remarks
1A (E-4051)	D-38 case, U-shaped grooves, half XTX	177.6	19.0	1.81	27.9	98	58.67	2.33	1
1B (E-4051)	D-38 case, V-shaped grooves, half XTX	186.1	19.0	1.55	23.9	120	58.67	2.33	
2A[a] (E-4076)	RTV-lined tungsten, U-shaped grooves	232.4 w/liner	17.3	0.54	8.4	426	59.94	2.72	2
2B (E-4076)	RTV-lined tungsten, U-shaped grooves	233.6 w/liner	17.3	0.55	8.5	426	59.44	2.72	
3A (E-4077)	Copper-matrix, tungsten-alloy spheroids	212.0	17.8 (spheroids)	0.26	4.01	500	58.00	3.60	3
3B (E-4077)	Lead-matrix, tungsten-alloy spheroids	243.6	17.8 (spheroids)	0.26	4.01	500	58.40	3.80	
4A (E-4078)	Tungsten grid screen, half XTX	226.2 (+ 6.4 for grid screen)	18.0	0.76	11.8	296	58.04	2.52	4
4B (E-4078)	Tungsten-alloy grid screen, half XTX	231.3 (+ 6.6 for grid screen)	17.9	0.78	12.0	296	58.17	2.61	
5A (E-4097)	Scored tungsten, half XTX	187.0	18.0	0.44	6.8	426	55.80	2.51	5
5B (E-4097)	Scored-tungsten alloy, half XTX	186.3	17.4	0.46	7.2	402	57.10	2.54	
6A (E-4094)	Copper-matrix, tungsten-alloy spheroids	213.7	17.8	0.26	4.01	500	58.00	3.66	3
6B (E-4094)	Lead-matrix, tungsten-alloy spheroids	238.8	17.8	0.26	4.01	500	57.40	3.71	

[a]The two hemishells of Test 2 were prepared identically; they are separated in the table to denote slight weight and scoring differences.

REMARKS

1. XTX pressed into the grooves of one-half of each case as indicated in the second column.
2. RTV liner 1.22 ± 0.2 mm thick, grooves 0.76 mm deep by 0.6 mm wide in both hemishells.
3. Tungsten-alloy (95 W/2.5 Ni/2.5 Fe wt%) spheroids with a nominal diameter of 3.05 mm.
4. One-half of each hemishell screen was filled with XTX.
5. XTX was pressed into the grooves of one half of each hemishell. The grooves were 1.27 mm wide by 0.6 mm deep in both hemishells. The tungsten hemishell was impregnated with ~0.2 g of copper to fill a circular crack at the polar end.

Tests 1 and 5 demonstrated the feasibility of controlling the fragmentation of heavy-metal cases (D-38 and tungsten/tungsten alloy, respectively) scored similarly to the steel case of the BLU-63 submunition (Figs. 2 and 3). Scoring differences and the effect of additional explosive (Extrudable Explosive, XTX-8003) in the grooves were also studied.

Test 2 demonstrated possible enhancement of fragmentation control and fragment velocity by inserting a room temperature vulcanized (RTV) silicone liner in a scored tungsten case (Fig. 4). Test results were compared with analogous results for the scored, pure tungsten quadrant of Test 5 containing no XTX in the grooves.

Test 3 and its repeat, Test 6, were performed to demonstrate the feasibility for controlling the fragmentation of selected heavy-metal fragments (tungsten-alloy spheroids) in a matrix of lighter case material (Fig. 5). Copper and lead matrices were studied. The packing of the spheroids in the lead matrix is shown in Fig. 6.

Test 4 studied the efficiency of controlling fragmentation of an unscored heavy-metal case (tungsten and tungsten alloy) by placing a copper-screen grid of desired size within each hemisphere (Fig. 7). The grid was to act as a fragmentation initiator.

III. EXPLOSIVE SYSTEM

The explosive system chosen for this study consisted of an electric detonator, a 280-mm- (11-in.) long mild detonating fuse (MDF), a 12.7-mm- (0.5-in.) diam sphere of XTX-8003 explosive, and a 50.8-mm- (2-in.) o.d. by 12.7-mm- (0.5-in.) i.d. spherical shell of plastic-bonded explosive, PBX-9404. The MDF passed through a hole in the PBX-9404 shell and into the XTX to a position that resulted in the generation of a spherically expanding detonation in the PBX-9404. The spherical detonation was slightly perturbed near the MDF.

This system was chosen because (1) A high-energy explosive was needed to achieve the desired high-fragment velocity. (2) The system is a well-characterized stock item and was, therefore, readily available and required no explosive development. (3) The spherically expanding detonation generated by the system is well approximated by 1D hydrodynamic calculations. This allowed inexpensive predetermination of experimental design parameters such as instrument activation times. (4) The spherically expanding detonation of this system, as opposed to the sweeping detonation in a conventional BLU-63, imparts a relatively higher early velocity to the metal case. This was desirable because the heavy-metal cases were expected to rupture at lower expansions than the steel case of the BLU-63. (5) The pressure gradient established by this system is greater than that caused by a sweeping detonation. Accordingly, if fragmentation can be controlled with this system it can also be controlled with a sweeping detonation; the converse is not necessarily true. (6) The uniform expansion of this system would make data interpretation particularly straightforward.

IV. EXPERIMENTAL ARRANGEMENT

The assembled explosive devices were suspended in the center of a partial arena similar to that shown in Fig. 8.

The threefold purpose of the arena was to (1) observe the fragmentation pattern, (2) recover some fragments, and (3) obtain some measure of penetration. The arena consisted of a 1.2-m cube with four closed sides, constructed of 19-mm (3/4-in.) plywood with 2 by 4 lumber supports. The sides and tops were a single layer of plywood. The bottom consisted of six layers of plywood in Tests 1-4 and eight layers in Tests 5 and 6. In Test 1, the bottom of the arena was covered with a 90-mm layer of water to quench burning of the pyrophoric D-38 fragments.

In Tests 2-4, arrival-time foils were placed on the inside of the two arena sides as a back-up measurement of velocity. They were placed with the understanding that it would be impossible to identify the size or nature of the fragment that actually tripped the foil.

Two film cassettes were placed on a wooden table within the arena, ~300 mm from the device, to obtain high-resolution flash radiographs of the fragments. They were placed symmetrically within the arena, perpendicular to direct lines drawn between the x-ray source units through the center of the test device. The case equator of the test device defined a plane that separated the two film cassettes. Each film cassette was protected with four layers of 12.7-mm-thick Lexan (a commercially available polycarbonate plastic). The arrangement allowed flash radiographs to be taken at two different times after detonation without superimposed images. A third film cassette, located inside the arena on the left, flush with and at the lower left-hand corner, allowed a late-time flash radiograph to be taken across the expanding shell of fragments. This cassette was protected by two layers of 12.7-mm-thick Lexan. This cassette was exposed by a third x-ray source unit located perpendicular to the cassette face and ~1.5 m distant. Steel plates were positioned in strategic locations around the arena to

prevent exposure of film cassettes by the wrong source unit. Figure 9 shows the experimental arrangement.

V. RESULTS

Examination of the plywood arena after each test allowed a measure of the fragmentation pattern and penetration. These results are summarized in Table II. The degree of fragmentation is evidenced by the relative number of holes in each arena piece. A measure of the degree of uncontrolled fragmentation is shown by the wide variation in hole sizes for a given hemishell. The relative penetration of the fragments (Fig. 10) is shown by the number of holes in the various bottom layers expressed as a percentage of the number of holes in the first bottom layer of the arena. Note that the various heavy-metal cases were designed to produce various numbers of fragments (refer to Table I).

In all but Test 3, flash radiographs were successfully taken of the expanding spheres of fragments at three different times after detonation (Radiograph 2 was lost in Test 3 because of an instrument malfunction). Figure 11 shows the flash radiographs obtained in Test 6. Time of first significant case motion was measured in all but Test 5. The time at which the flash radiographs were taken

TABLE II

FRAGMENT PENETRATION DATA

NUMBER OF ENTRY HOLES

Fragmentation by Hemishell Penetration Area	Test 1 (E-4051) Scoring D-38	Test 2 (E-4076) Scoring RTV/Liner Tungsten	Test 3 (E-4077) Tungsten-Alloy Spheroids Lead[g]	Test 3 (E-4077) Tungsten-Alloy Spheroids Copper[g]	Test 4 (E-4078) Screen Grid Pure Tungsten	Test 4 (E-4078) Screen Grid Alloy	Test 5 (E-4097) Scoring Pure Tungsten	Test 5 (E-4097) Scoring Alloy	Test 6 (E-4094) Tungsten-Alloy Spheroids Lead[g]	Test 6 (E-4094) Tungsten-Alloy Spheroids Copper[g]
Arena[a] Top	51	155	89	455	236[h]	197[h]	227[h]	447[h]	92	320
Arena Left Side[b]	29	158	204	---	---	366[l]	---	269[l]	165	---
	---	---	---	---	---	183[h]	---	265[h]	---	---
Arena Right Side[b]	30	154	---	401	286[l]	---	242[l]	---	---	404
	---	---	---	---	160[h]	---	293[h]	---	---	---
Arena Bottom No. 1[c]	37[f]	148	92	218	391[l]	409[l]	251[l]	387[l]	92	222
Arena Bottom No. 2	32	117	78	103	143[l]	251[l]	126[l]	204[l]	92	65
Arena Bottom No. 3	20	103	77	49	36[l]	177[l]	69[l]	154[l]	78	48
Arena Bottom No. 4	12	86	63	42	8[l]	69[l]	49[l]	93[l]	69	30
Arena Bottom No. 5	2 dents	75	60	29	2[l]	18[l]	24[l]	21[l]	61	17
Arena Bottom No. 6	0	53	47	16	0[l]	5[l]	8[l]	1[l]	46	9
Arena Bottom No. 7[d]	---	---	---	---	---	---	0[l]	0[l]	20	3
Arena Bottom No. 8[d]	---	---	---	---	---	---	0[l]	0[l]	0	2
Design[e]	36	143	84	84	49	49	71	67	84	84
Remarks	1	2	3	3	4	4	4	4	5	5

[a] Each arena piece was 19-mm (3/4-in.) plywood.

[b] Sides partially masked by film cassettes.

[c] Bottom arena piece closest to the device.

[d] Tests 5 and 6 only.

[e] Approximate number of fragment penetrations in arena bottom section if perfect fragmentation occurred.

[f] Arena bottom covered by 90 mm of water.

[g] The first layer of the arena on the copper side sustained damage from matrix material as well as spheroids; the counted holes range down to pinhole size. The first four bottom layers sustained holes up to 12.7-mm diam on the copper side. Counted holes on the lead side include only the > 2-mm holes obviously attributable to the tungsten-alloy spheroids.

[h] Without XTX treatment, Tests 4 and 5 only.

[l] With XTX treatment, Tests 4 and 5 only.

REMARKS

1. There were no apparent penetration differences from the four different groove treatments. Counted holes were 3.2 mm or greater in minimum dimension.
2. Approximately 14 penetrations in ground beneath Bottom No. 6. Counted holes were 3.2 mm or greater in minimun dimension.
3. Greater damage on the copper side and greater penetration on the lead side. Approximately 20 spheroids from the lead side penetrated the ground beneath Bottom No. 6.
4. No predominance of a particular size hole was evident. Counted holes range down to pinhole size.
5. On the copper side, two spheroids penetrated below Bottom No. 8, ~3 cm into the ground.

and the time of first significant case motion were recorded. A knowledge of the initial case radii and measurements of the fragment radii at the flash radiograph times allowed calculation of the average fragment velocity over several flight paths. These velocity measurements contain inherent uncertainties. In some instances it was very difficult, because sufficient expansion had not occurred, to determine the outer perimeter of the important fragments (those of a lethal size, i.e., >0.25 g or 4.0 grains) in Radiographs 1 and 2. The positioning of film cassette No. 3 made it impossible to determine with accuracy the identity of fragments, their precise distance from the center of detonation, and the portion of the expanding shell of fragments with which a particular fragment could be associated. For those tests where an arrival time foil (armored with 12.7 mm of Lexan) was used, the foil gave an anomalously high velocity; this was probably caused by unimportant high-velocity, low-weight fragments. Velocities calculated from arrival time foils have, therefore, been excluded from consideration. Velocities are summarized in Table III. Except in Test 6, there were no significant velocity differences noted for the various heavy-metal case/explosive configurations involved within each test. A plot of the weight ratio (weight of case/weight of high explosive) is given in Fig. 12.

Partial recovery of fragments from the six test shots was made from various areas of the arena and from the polycarbonate layers (Lexan) that protected the film cassettes. The weight distributions of the recovered fragments are given in Table IV. In no case was complete fragment recovery attempted. Therefore, unless otherwise noted, the weights given in the table are not necessarily a representative sample of fragments from that location. A lack of recovered fragments from a particular location does not denote the absence of fragments unless specifically noted. For each recovery location, three qualities are given: (1) weight range in grams, (2) average weight in grams, and (3) number of fragments recovered.

An analysis of the flash radiographs and arena pieces resulted in a qualitative description of the fragmentation of all test devices.

Test 1. The D-38 hemishells clearly ruptured along the scored grooves in all quadrants, producing lethal-sized fragments. Essentially all of the smaller fragments were produced from the regions of the grooves. No significant fragmentation differences

TABLE III

VELOCITIES[a] OF LETHAL FRAGMENTS

OVER DIFFERENT FLIGHT PATHS

Flight Path	Test 1 (E-4051) Largest Fragments	Test 1 (E-4051) 1- to 3-mm Fragments	Test 2 (E-4076)	Test 3 (E-4077) Lead	Test 3 (E-4077) Copper	Test 4 (E-4078)	Test 5 (E-4097)[d]	Test 6 (E-4094) Lead	Test 6 (E-4094) Copper
First significant motion to Radiograph 1	0.98 (3215)	1.55 (5085)	1.28 (4199)	1.29 (4232)	1.30 (4265)	1.24 (4068)	---	0.98 (3215)	1.20 (3937)
First significant motion to Radiograph 2	1.22 (4002)	1.82 (5970)	1.25 (4101)	---	---	1.30 (4265)	---	1.00 (3281)	1.23 (4035)
First significant motion to Radiograph 3[b]	---	---	1.30 (4265)	1.61 (5282)	1.61 (5282)	1.08 (3543)	---	1.28 (4199)	1.29 (4232)
Radiograph 1 to Radiograph 2	---	1.80 (5905)	1.36 (4462)	---	---	1.34 (4396)	1.48 (4856)	1.04 (3412)	1.29 (4232)
Radiograph 1 to Radiograph 3[b]	---	---	1.31 (4298)	1.62 (5315)	1.62 (5315)	1.08 (3543)	1.59 (5216)	1.31 (4298)	1.29 (4232)
Radiograph 2 to Radiograph 3[b]	---	---	1.30 (4265)	---	---	1.05 (3445)	1.60 (5249)	1.33 (4363)	1.29 (4232)
Representative fragment weight (grains)	25	1-7	8	4	4	---	0	4	4
Remarks	1	1		2	2				

[a] Velocity in mm/μs (ft/s in parentheses).

[b] This velocity may be in error by as much as +40% because fragment distances in Radiograph 3 are not accurately known.

REMARKS

1. In Radiograph 1, lethal-size fragments were obscured by fine particles. Hence, the velocity of fragments is biased low.
2. By the time of Radiograph 1, tungsten-alloy spheroids could not be discerned from matrix material. Radiograph 2 was lost, hence velocities are biased.

TABLE IV

FRAGMENT WEIGHTS AS A FUNCTION OF RECOVERY LOCATION [a]

Hemishell	Test 1 (E-4051) 0-38	Test 2 (E-4076) Tungsten	Test 3 [b] (E-4077) Lead	Copper
Recovery Area:				
Arena Top	1	1	2	2
Arena Left Side	1	1	2	2
Arena Right Side	1	1	2	2
Bottom No. 1 [c]	0.0130-0.0350; 0.0240 (2)	1	2	2
Bottom No. 2	0.4984-0.9138; 0.7343 (3)	1	0.2604; 0.2604 (1)	1
Bottom No. 3	0.8120-0.8671; 0.8396 (2)	0.1402; 0.1402 (1)	0.2615: 0.2615 (3)	1
Bottom No. 4	0.5172-0.9034; 0.7686 (3)	0.1544-0.5821; 0.3270 (6)	1	1
Bottom No. 5	---	0.2640-0.8964; 0.4898 (10)	0.2573-0.2735; 0.2660 (3)	0.2328; 0.2328 (1)
Bottom No. 6	---	0.0888-0.5848; 0.3004 (6)	0.2661; 0.2661 (1)	0.2420; 0.2420 (1)
Bottom No. 7 [d]	---	---	---	---
Bottom No. 8 [d]	---	---	---	---
Lexan 1A [e]	1	1	1	---
Lexan 1B	0.0298-0.3402; 0.1850 (2)	1	1	---
Lexan 1C	0.0881-0.7298; 0.4850 (3)	0.2758-0.5062; 0.3910 (2)	0.2540-0.2695; 0.2644 (6)	---
Lexan 1D	0.5120; 0.5120 (1)	0.4051-0.6122; 0.4768 (4)	0.2601; 0.2601 (1)	---
Lexan 2A [e]	No recovery attempted	1	---	Matrix material only
Lexan 2B	No recovery attempted	1	---	Matrix material only
Lexan 2C	No recovery attempted	0.0443-0.4253; 0.2832 (6)	---	0.2107-0.2501; 0.2258 (6)
Lexan 2D	No recovery attempted	0.1860; 0.1860 (1)	---	0.2134-0.2397; 0.2228 (8)
Lexan 3A [e]	No recovery attempted	1	1	---
Lexan 3B	No recovery attempted	1	0.2627-0.2784; 0.2705 (2)	---
Other	Water tank 0.6481-0.8036 0.7511 (4)	Ground 0.3092-0.6590; 0.5232 (8)	Ground 0.2550-0.2560; 0.2555 (2)	2
Remarks	3	4	5	5

[a] Figures given for each test have the weight range on the first line and the average weight and number of fragments (in parentheses) below.

[b] Weights are for spheroids and attached matrix material; not matrix material alone.

[c] No. 1 was closest to the device.

[d] These layers present in Tests 5 and 6 only.

[e] The numeral of each 12.7-mm-thick Lexan sheet denotes the associated flash radiograph machine; the alphabetic characters denote nearness to the device in the order A, B, C, and D.

REMARKS

1. No significant fragment found.
2. Definitely no fragments present.
3. Fragments evidenced burning. No distinction between groove treatments.

Test 4 (E-4078)		Test 5 (E-4097)		Test 6[b] (E-4094)	
Pure Tungsten	Alloy	Pure Tungsten	Alloy	Lead	Copper
Too small to recover	Too small to recover	1	1	2	2
Too small to recover	Too small to recover	1	1	2	2
Too small to recover	Too small to recover	1	1	2	2
0.0036-0.0072; 0.0045 (5)	0.0069-0.1019; 0.0699 (3)	1	1	2	2
0.0154-0.0238; 0.0197 (2)	0.0551-0.0723; 0.0623 (4)	Fine particulate matter only		0.2570; 0.2570 (1)	1
0.0229; 0.0229 (1)	0.0023-0.1122; 0.0540 (8)	0.0810-0.1750; 0.1066 (5)	0.1128-0.1828; 0.1478 (2)	0.2032; 0.2032 (1)	1
0.0042-0.0504; 0.0291 (3)	0.0199-0.1748; 0.1060 (8)	0.1423; 0.1423 (1)	0.1374-0.1964; 0.1674 (5)	1	1
1	0.1097-0.1591; 0.1324 (3)	0.1755-0.2964; 0.2360 (2)	0.1070-0.1898; 0.1616 (4)	0.2594-0.2629; 0.2612 (2)	0.2289; 0.2289 (1)
1	0.1792; 0.1792 (1)	0.0785-0.2000; 0.1392 (2)	1	0.2557-0.2664; 0.2605 (5)	0.2079-0.2883; 0.2379 (7)
---	---	2	2	0.2605-0.2663; 0.2628 (4)	0.2597-0.2805; 0.2734 (3)
---	---	2	2	2	2
---	2	---	Fine particle matter only	1	---
---	0.0839-0.1191; 0.1068 (4)	---	0.1644; 0.1644 (1)	1	---
---	0.0390-0.2040; 0.1272 (7)	---	0.1840-0.2518; 0.2220 (3)	0.2571-0.2736; 0.2636 (7)	---
---	0.1865-0.9321; 0.5593-(2)	---	0.0797; 0.0797 (1)	0.2616-0.2654; 0.2625 (3)	---
2	---	Fine particle matter only	---	---	2
Too small to recover	---	0.1125-0.1857; 0.1376 (3)	---	---	0.3234; 0.3234 (1)
0.0165-0.1677; 0.0852 (3)	---	0.0608-0.2555; 0.1627 (9)	---	---	0.1800-0.2934; 0.2341 (7)
2	---	0.4086-0.4197; 0.4142 (2)	---	---	0.2054-0.2777 0.2283 (7)
---	1	---	1	1	---
---	0.0426-0.0773; 0.0656 (3)	---	0.1667; 0.1667 (1)	0.2608; 0.2608 (1)	---
---	---	---	---	Ground:c	0.1910-0.2750 0.2330 (2)
6	6	7	7	8	8

REMARKS (Cont)

4. Holes scorched. All fragments well defined.
5. Pieces of copper-matrix material weighing up to 0.4210 g recovered from as deep as Bottom No. 3. Spherold in Lexan ID was only one evident at this level.
6. All but two fragments (0.2040 g, 0.9321 g) were poorly defined.
7. Much fine particulate matter (0.0638 g or less) associated with all layers. Above tabulation includes only the well-defined fragments.
8. Pieces of copper-matrix material weighing up to 0.4736 g recovered from as deep as Bottom No. 4. Lexan 10 had three imbedded lead-matrix spherolds, Lexan 20 had ~30 imbedded copper-matrix spherolds.

were noted between the four different groove treatments, i.e., U- and V-shaped grooves, filled or not filled with XTX. The fragmentation pattern was orderly and well defined; penetrations of lethal-sized fragments were clearly distinguishable from those made by the smaller fragments. Recovered fragments show evidence of burning. Larger recovered fragments appear to have been quenched by water or Lexan. Fragments penetrated as far as bottom layer No. 5. The design of D-38 fragments was such that they had a signficantly greater area-to-thickness ratio and were heavier than any other test fragment.

Test 2. The scored-tungsten case with RTV liner fragmented along the machined grooves with essentially no additional fragmentation. Fragments penetrated deeply, some passing through six layers of 19-mm (3/4-in.) plywood and 50 mm (2 in.) of hard-packed sandy soil. Recovered fragments were well defined (as per case scoring) and apparently not deformed.

Test 3. The important fragments from both matrices were the tungsten-alloy spheroids. The lead matrix vaporized early in the expansion and did not significantly contribute to the arena damage. The copper-matrix material clung to the tungsten-alloy spheroids and also fragmented, particularly in the equatorial region. (The increased fragmentation near the equator appears to be related to the greater amount of matrix material in this region.) Tungsten-alloy spheroids from the lead matrix were recovered with no deformation; those from the copper matrix had copper attached and were slightly spalled. The fragment pattern from the lead hemishell was well ordered; spheroid penetrations were of uniform size and surrounded by a fine spray of superficial penetrations. The fragment pattern from the copper hemishell was less orderly; there was a wide range of penetration sizes (12.7 mm down to pinhole) resulting from spheroids and fragments of copper alone. Spheroids from the lead matrix penetrated to a depth of 10 mm into a steel boiler plate located 610 mm from the center of detonation. Generally, spheroids from the lead matrix were more penetrative; fragments from the copper matrix were more destructive.

Test 4. By 22 μs after first significant case motion, the heavy-metal case had clearly ruptured along the lines defined by the enclosed screen grid. However, by 60 μs after first significant motion it was apparent that significant, additional fragmentation had occurred. Little fragmentation difference was evident between the pure tungsten and tungsten-alloy hemishells. However, the XTX-treated half of the sphere did show approximately twice as many fragments as the nontreated half. Alloy fragments were more penetrative than pure tungsten fragments. Recovered fragments fell into two categories: (1) well defined, obviously fragmented along the grid screen, or (2) portions of defined fragments or groove material. Tungsten fragments penetrated as far as bottom layer No. 5, alloy fragments as far as bottom layer No. 6.

Test 5. Although the first radiograph showed clear rupture along the scored grooves, considerable additional fragmentation was evident by the time of the second radiograph. The XTX treatment of half of each hemishell did not affect fragmentation. However, the alloy hemishell showed approximately twice as many fragments as the tungsten hemishell. Furthest penetration was to bottom No. 6; the pure tungsten hemishell produced slightly more penetrative fragments. Recovered fragments included both well-defined ones and poorly-defined chips.

Test 6. All observations made in Test 3 were confirmed in this test. Steel boiler plates were located on each side of the arena, 610 mm from detonation center. The plate on the lead-matrix side showed an orderly pattern of 10-mm-deep penetrations, whereas the plate on the copper-matrix side showed a reltively disorderly array of 10-mm-deep penetrations made by the spheroids and additional scattered, superficial damage done by matrix material.

VI. HYDRODYNAMIC CALCULATIONS

To facilitate selection of meaningful experimental parameters, such as explosive fill and case thickness, SIN 1D hydrodynamic calculations[1] were performed for various combinations of explosive fill and case material. These calculations did not treat fragmentation. Therefore, material combinations were sought that would achieve the desired minimum velocity of 1 mm/μs within the expansion achieved by a conventional BLU-63 when the case ruptured. Case rupture for this device with preferred fill occurs when the case radius has been increased by about 12 mm. After case rupture some additional acceleration of fragments can be expected, but not as much as the calculations predict. Table V summarizes the calculations performed which were subsequently used to develop our experimental scheme.

The equation-of-state parameters for case materials were as follows.

Parameters	Material			
	Steel	Tungsten	Neoprene	Copper
ρ	7.917	19.17	1.439	8.903
C	0.458	0.4005	0.2785	0.3958
S	1.51	1.268	1.419	1.497
γ	2.0	1.54	1.39	2.0
Cv	0.107	0.092	0.20	0.093
$\alpha \times 10^{-5}$	1.17	1.0	1.0	1.767

The calculated free-surface velocity (in mm/μs) and outer radius (in mm) of the outer case are plotted for selected problems as a function of time (in μs) in Figs. 13-22.

Assuming that the calculated velocities at an expansion of 12 mm are equivalent to the terminal velocities in the experiments, Fig. 33 plots the predicted terminal velocities for the calculated systems as a function of case weight/HE weight. The calculated velocities for problems T-188, T-178, and T-179 show the effect of increasing the explosive energy (Amatex 20, Composition B, and PBX-9404, respectively).

VII. FABRICATION PROCEDURES FOR HIGH-DENSITY METAL FRAGMENTATION CASES

Several methods, individually described below, were used to fabricate fragmentation hemishells or cases for this study. Tungsten and tungsten-alloy shells were made using a multistep process which involved isostatic compression, presintering, machining, and sintering. The uranium shells were made by scoring sheet stock followed by deep drawing. The shells containing tunsten-alloy spheroids in matrices of copper or lead were made using a casting process. The shell dimensions were 50.8-mm-i.d. with a 2- to 3.5-mm wall thickness.

In addition to the hemishells, fragmentation initiators in the form of hemispherical screens and grids were fabricated from copper and steel using etching and deep drawing techniques.

A. Tungsten and Tungsten-Alloy Fragmentation Shell Fabrication

1. **Tungsten Hemishells.** Four tungsten hemishells were fabricated for the fragmentation tests using an isostatic pressing process. Two of these shells were used in Test 2 and were made from a 5-μm Fisher subsieve-size General Electric tungsten powder designated W-195. Table VI shows the results of the chemical analysis and particle size measurements of this powder and the other

TABLE V

EXPERIMENTAL HYDRODYNAMIC CALCULATIONS

Calculation Symbol	High Explosive	HE Radius (mm)	Inner Case	Thickness (mm)	Outer Case	Thickness (mm)
T-178	Comp. B	25.908	(none)	---	Steel	3.302
T-179	PBX-9404	25.908	(none)	---	Steel	3.302
T-180	Comp. B	25.908	(none)	---	Tungsten	3.302
T-181	PBX-9404	25.908	(none)	---	Tungsten	3.302
T-182	PBX-9404	25.324	Copper	1.092	Tungsten	2.794
T-184	PBX-9404	26.416	(none)	---	Tungsten	2.794
T-185	PBX-9404	25.324	Neoprene	1.092	Tungsten	2.794
T-186	PBX-9404	24.740	Neoprene	2.184	Tungsten	2.286
T-188	Amatex 20	25.908	(none)	---	Steel	3.302
T-190	PBX-9404	27.560	(none)	---	Tungsten	1.650

TABLE VI

CHEMICAL ANALYSES AND AVERAGE PARTICLE SIZE OF

IRON, NICKEL, AND TUNGSTEN POWDERS

AND TUNGSTEN ALLOY

Lot Number	Fe-31	Ni-27	W-195	W-180	Tungsten Alloy
C	380[b]	---	---	---	---
O	1600	---	438	2915	---
Li	< 10	< 4	---	---	< 1
Be	< 10	< 4	---	---	< 1
B	< 100	< 10	---	---	< 1
Na	< 30	< 4	---	---	< 13
Mg	< 3	1	< 3	< 3	1
Al	< 10	< 8	< 6	< 6	13
Si	< 3	< 10	10	7	< 13
K	< 30	< 20	---	---	< 13
Ca	< 10	< 1	25	13	6
Ti	< 10	< 8	---	---	< 13
Cr	10	< 4	7	4	6
Mn	< 3	< 4	< 6	< 6	3
Co	< 10	< 40	---	---	< 4
Ni	100	---	5	3	3.31%
Cu	< 10	10	10	3	26
Zn	< 100	< 100	---	---	< 130
Sr	< 10	< 8	---	---	< 1
Zr	< 100	---	---	---	< 130
Nb	< 300	---	---	---	< 0.13%
Mo	< 100	---	256	22	< 130
Cd	< 10	---	---	---	< 1
Sn	< 30	---	< 6	< 6	< 13
Ba	< 10	---	---	---	< 1
Fe	---[c]	< 10	36	3	1.50%
W	---	---	---	---	95.0%
APD[a]	7.9[d]	11.7[d]	5.0[e]	0.64[e]	---

[a]Average particle diameter, μm.

[b]Values expressed as parts per million unless otherwise indicated.

[c]Element not determined.

[d]Measured with a sedibalance.

[e]By Fisher sub sieve sizer per ASTM B-330.

tungsten, tungsten-alloy, iron and nickel powders used in this study.

The remaining tungsten shells, one used in Test 4 and one in Test 5, were made with a General Electric tungsten powder, designated W-180, which had a considerably smaller, 0.64-μm, Fisher subsieve particle size.

Tungsten hemishells were prepared by isostatically pressing the powder over a male aluminum hemispherical-shaped mandrel using the arrangement shown in Fig. 34. The mandrel was somewhat larger than the desired inside diameter of the finished part to allow for shrinkage during sintering.

The mandrel was placed into a pressing sack made of polyvinylchloride plastisol (Chem-o-sol No. PK1088 from Chemical Products Corporation) and the sack was loaded with tungsten powder. A plastisol lid was sealed to the sack using a thin syrup made of plastisol dissolved in methylethylketone. The green pressing was made in an Autoclave Engineering Isostatic Press using a pressure of 345 MPa with oil as the pressure medium.

After removal from the pressing chamber, the green preforms were presintered at 1175 K in hydrogen for a minimum of 2 h. At this stage the tungsten had enough strength for ease of handling and machinability. The tungsten hemishells that required scoring on their inner surface for purposes of fragmentation initiation were machined at this stage.

Final sintering procedures varied somewhat for the different hemishells. Those used for Test 2 were sintered in hydrogen for 2 h at 1975 K followed by a vacuum treatment (6.65 MPa) at 2475 K. Figure 35 shows a tungsten preform and a finished tungsten hemishell. The immersion densities of 17.3 g/cm^3, or 90% of the theoretical value, were lower than anticipated; insufficient shrinkage left the shell slightly oversized. Consequently, these shells were used for the RTV rubber-liner experiments for Test 2.

The hemishells used in Tests 4 and 5 were made with the finer tungsten powder. They were sintered at 1975 K in hydrogen for 4 h. The shell used in Test 5 was sintered an additional 2 h in vacuum at 2475 K. The Test 4 case had an immersion density of 18.02 g/cm^3.

During sintering, the Test 5 hemishell developed a small circular crack at the pole which was repaired by impregnating it with copper at 1455 K. It had a density of 17.96-g/cm^3 after repair. Radiographic inspection indicated that the copper had impregnated the crack successfully and that there were no openings through the case walls.

Figures 36 and 37 are photomicrographs of tungsten control specimens that were carried through the process in an identical manner to the hemishells. The sample given the additional 2-h vacuum treatment at 2475 K had a slightly larger grain size, 32 μm, as compared with 22.4 μm for the sample sintered at 1975 K. A slight decrease in porosity also seems to have occurred during the additional sintering, although the density figures do not show this. The discrepancy is undoubtedly caused by the impregnation of a crack in the Test 5 hemishells with copper, which would cause the piece to have a lower density than a solid tungsten piece.

2. Tungsten-Alloy Hemishells. Tungsten-alloy hemishells were used to form one-half of the fragmentation cases for Tests 4 and 5. The alloys were made using the 5-μm tungsten powder (W-195); a nickel powder, Ni-27, obtained from the ALCAN Company; and an iron powder, Fe-31, obtained from the General Aniline and Film Corporation.

The chemical analysis and particle size of the starting materials are given in Table VI. The nominal composition of the tungsten alloy was 95 wt% tungsten, 3.5 wt% nickel, and 1.5 wt% iron. The actual composition of the sintered hemishells as determined by chemical analysis is also shown in Table VI. It was very close to nominal values.

In general, the same procedures were used to make the tungsten-alloy hemishells as were used to make the all-tungsten cases, therefore only the differences will be discussed.

Prior to loading the pressing sacks, the tungsten-nickel-iron mixtures were blended in a twin-shell blender for 8 h. Identical isostatic pressing procedures to those used for the tungsten parts were followed. The grooves designed to control the fragmentation pattern were machined into the inside surface of the hemishell used for Test 5 after presintering. The shells for Tests 4 and 5 were rough-machined, making allowance for shrinkage while in the presintered state. The outside diameters were machined to the final size after the liquid-phase sintering operation.

The tungsten alloy, a liquid-phase sintering material, was sintered in hydrogen for 2 h at 1675 K followed by 1 h at 1735 K for a total of 3 h. Again, control specimens were carried throughout the operation under identical conditions as the part. Figure 38 shows the microstructure of the sintered tungsten-alloy samples. The structure is typical of liquid-sintered tungsten containing the nearly spherical tungsten grains surrounded by a matrix of nickel-iron-tungsten alloy.

B. Fabrication of D-38 Fragmentation Hemishells

Test 1 of this series used a D-38 case made of two uranium hemishells, one with machined V-grooves and one with U-grooves. The hemishells were formed by rolling a uranium sheet to a 3.81-mm thickness and cutting 87.3-mm-diam blanks from the sheet. These blanks were then scored on one side with either V- or U-shaped grooves and deep drawn into hemishells with the grooves on the inside. The deep-drawing operation was carried out at 475 K using a punch with a 50.96-mm-diam hemispherical tip and a die with a 58.87-mm-diam cavity.

The deep-drawn hemishells were finished by machining off the excess to an inside pole height of 25.4 mm. The drawing blanks and the finished uranium hemishells are shown in Fig. 39. These scored hemishells are easy to form and the process could readily be adapted to a high-speed production process.

C. Fabrication of Fragmentation Hemishells of Tungsten-Alloy Spheroids in Copper and Lead Matrices

Tungsten-alloy spheroids having a nominal composition of 95 wt% tungsten, 2.5 wt% nickel, and 2.5 wt% iron were purchased from the Kulite Tungsten Corporation. The spheroids had a density of 17.8 g/cm^3, a diameter of 3.05 mm, and weighed about 0.26 g/sphere. A small flash was observed around the equator of the spheroids, evidently from the die-pressing operation used to form the spheroids from metal powders. Figure 40 shows the microstructures of the spheroids; it is similar to the 95 wt% tungsten-3.5 wt% nickel-1.5 wt% iron alloy structure, shown in Fig. 38, that was used for Tests 4 and 5. Pig lead, corroding high purity, from Dixie Industries and oxygen-free high conductivity (OFHC) copper were used as matrix material for these hemishells.

A casting procedure was used to fabricate the fragmentation shells containing tungsten-alloy spheroids. Castings were made using lead and copper as matrix materials. The casting operations were conducted in a LASL-designed and constructed induction-powered casting furnace using an air atmosphere for the lead-matrix hemishells and vacuum for the copper-matrix hemishell.

The castings were made in a graphite mold (Fig. 41) that consisted of (1) the outer case, which contained a cavity conforming to the outside diameter of the hemishell; (2) the runner box used to melt and feed the matrix metal; and (3) a core, which determined the inside diameter of the hemishell. The core was press-fit into the runner box to hold it in place during handling and casting operations.

The tungsten-alloy spheroids were weighed (~500 spheroids made a charge) and placed in the mold cavity wall between the outer diameter of the core and the inner diameter of the mold as shown in Fig. 41. The mold was vibrated for 2 min to obtain good packing.

The charge, either copper or lead, was placed in the runner box, which was slotted in three places to provide passage of the liquid melt into the mold. The mold was heated inductively to 1525 K for copper and 775 K for lead. As the material melted it flowed into the mold cavity around the spheroids. Temperature was maintained for 10 min to ensure complete penetration around the spheroids in the mold.

After cooldown the mold was disassembled and the hemishell, core, and runner box were mounted in a lathe (by gripping the runner box), and the hemishell was parted at the equatorial line. Cores used for making copper-matrix material could only be used once; however, the cores used with the lead could be salvaged for reuse because of the lower shrinkage encountered. This casting process is an easy way to make fragmentation hemishells and could be adapted to a production process.

D. Fragmentation Initiators

The problem of providing fragmentation initiation was approached from several directions. As already discussed, fragmentation initiation for Tests 1, 2, and 5 was provided by machining grooves before deep drawing for the uranium cases and after presintering for the tungsten and tungsten-alloy cases. This was easy for the uranium, which was machined as a flat sheet, but slow for the tungsten and tungsten alloys, which were machined in the hemispherical shape. Consequently, another way was examined for grooving the tungsten and tungsten alloys—electrochemical etching.

An investigation of electrochemical grooving methods was carried out using flat plates of tungsten and tungsten alloy. The plates were nickel plated and a grid pattern placed on the surface by photolithography using Kodak photoresist. The grid lines were chemically etched through the nickel plate, exposing the tungsten. With the remaining nickel protecting the tungsten, the grooves were electrochemically etched in the unprotected grid pattern using a 2-kmol/m^3 (113-g/ℓ) solution of potassium hydroxide for tungsten and a concentrated solution of hydrofluoric acid for the tungsten alloy. Feasibility of this method was established, but was not used

to prepare cases for the tests because of expense and time delay in obtaining the necessary artwork needed to groove a hemispherical shell internally.

Test 4 used a copper-grid screen between the case and explosive to cause fragmentation initiation in the desired pattern. These were fabricated by laying out the pattern on 0.76-mm-thick circular copper blanks using Kodak photoresist. The grid was partially etched with a 3.39-kmol/m^3 (550-g/ℓ) solution of ferrichloride leaving the unprotected metal (where the holes in the grid would be) about 0.48 mm thick. At this stage the blank was deep drawn to form the hemispherical shape and the etching repeated to form the grid. The partially etched deep-drawn hemisphere is shown in Fig. 42. Attempts to form these grids after treating with photoresist, but without the preliminary etching treatment, failed because the photoresist rubbed off during the drawing operation.

Deep drawing a hemispherical shape from a copper screen appeared to be the easiest way to form the fragmentation initiators; however, all attempts using copper screen were unsuccessful because of wire breakage during drawing. Protecting the screen with an aluminum waster-plate during drawing did not prevent the screen from separating. However, a commercial steel screen with an 0.64-mm-thick web and a 12.7-mm-square opening was readily cupped directly into hemispheres. Figure 43 is a photograph of a steel blank and three cupped steel screen hemispheres. Steel would appear to be a better choice than copper for screen-fragmentation initiators from the viewpoint of materials cost and ease of fabrication.

VIII. SUMMARY AND CONCLUSIONS

Six heavy-metal fragmentation submunitions were fabricated and test fired. A scored D-38 case and a case consisting of tungsten-alloy spheroids in a lighter metal matrix proved easiest to fabricate. Three of the devices, a scored D-38 case, a scored tungsten-alloy case with an RTV liner, and tungsten-alloy spheroids in a lighter matrix material, achieved significantly greater penetration than a larger, similarly configured, conventional submunition, the BLU-61. Other test devices, scored and unscored tungsten and tungsten alloy without RTV liner cases, did not perform as well as the above devices. Their performance may be significantly improved by varying fabrication parameters such as grooving or screen-thickness depth. Overall, the tungsten-alloy spheroids in a lighter matrix material appear to be the superior system. However, study of the D-38 system was inadequate and cost considerations suggest, or may dictate, further investigation.

IX. RECOMMENDATIONS

Ease of construction, desirable fragment shape, and large number of fragments of the spheroid and matrix design suggest that the tungsten-alloy, light matrix design should be studied in detail, especially if investigation of the D-38 system is discontinued. The objects of the recommended study are twofold: (1) to characterize the spheroid and matrix design for determination of its applicability to present and future needs and (2) to determine whether the pyrophoric property of D-38 fragments offers a significant advantage.

The recommended study should include the effects of (1) spheroid mass, (2) explosive energy and radius, (3) method of initiation, (4) metal vs plastic aerodynamic case, (5) matrix and spheroid materials, (6) practical ways to achieve the desired equatorial mass, (7) multiple layer of spheroids, and (8) liner materials. This study should be closely coupled with lethality calculations based on weight and volume limits. However, lethality calculations should not dictate the experiments because weight and volume limits and targets may change in the future. Cost effectiveness and explosive energy requirements suggest that pressed explosives should be considered.[2]

Future needs suggest that a cylindrical submunition should be included in the study. This and other parts of the recommended study not requisite for present needs could be deferred.

We also recommend that the fragmentation properties of grooved D-38, and possibly of D-38 spheroids, be studied. Minimally, limited experiments to evaluate the benefits of its pyrophoric properties should be conducted. For example, it would be well to determine the consequence of D-38 fragment attack on containers of diesel fuel.

ACKNOWLEDGMENTS

We acknowledge the contributions of J. LaBerge, W. Morton, E. Viramontes, and H. Langley for test firing the explosive devices, and Charles L. Mader and R. Swanson for the theoretical studies. Harold Lootens, AMSAA, provided guidance and helpful discussions.

We also acknowledge the contributions of Harry Flaugh and his coworkers for the preparation and fabrication of the explosive charges. Our thanks to James F. Muller, Gale S. Hanks, Anton Mayer,

James Dickinson, and the many CMB-6 technicians for their assistance in fabricating various test bomblets used in this study. Our special thanks to Mr. George Jaynes who developed the method used for casting tungsten-alloy balls into soft-metal matrices at the suggestion of H. Lootens.

REFERENCES

1. Charles L. Mader and William R. Gage, "FORTRAN SIN. A One-Dimensional Hydrodynamic Code for Problems which Include Chemical Reactions, Elastic-Plastic Flow, Spalling, and Phase Transitions," Los Alamos Scientific Laboratory report LA-3720 (1967).

2. T. M. Benziger, "Press-Formed Explosive Charges for the BLU-26/B Fragmentation Bomb," Los Alamos Scientific Laboratory report LA-3779-MS (August 1967).

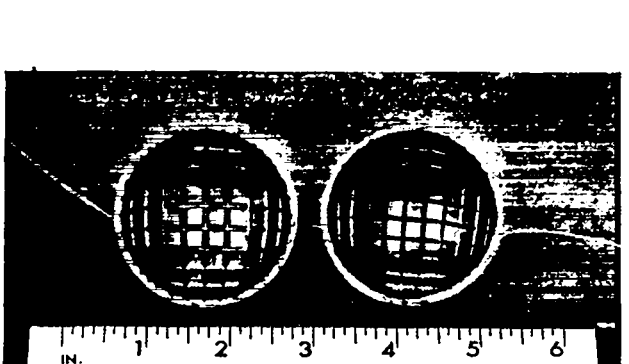

a. Detail of the groove patterns in the two D-38 hemishells.

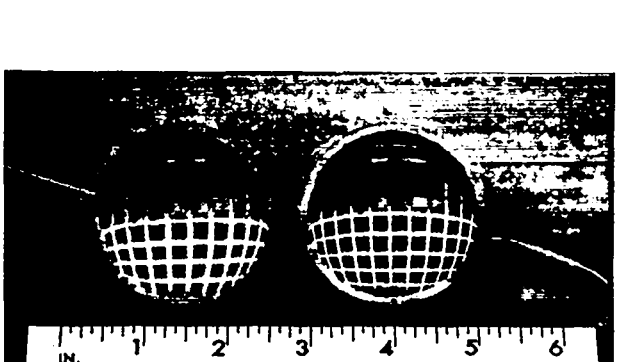

b. XTX pressed into grooves of one-half of each hemishell.

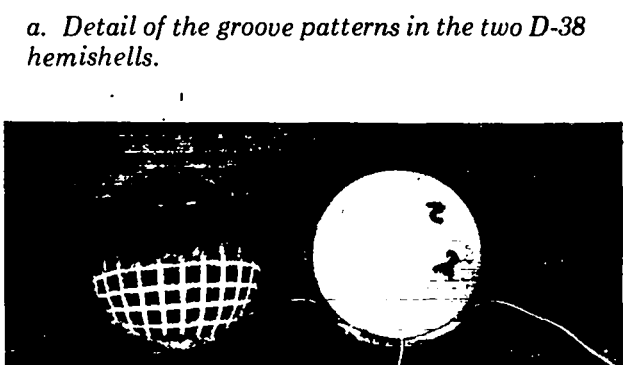

c. *PBX-9404 sphere placed in one-half of the D-38 case.*

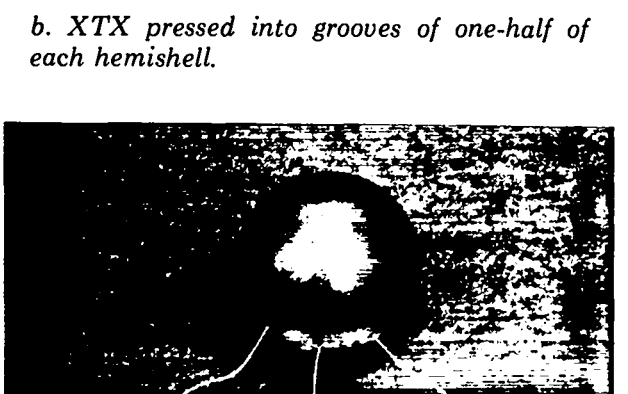

d. Assembled device, ready to fire. The wires to the left and right are for suspending the charge.

Fig. 1.
Assembly procedure for Test 1 firing.

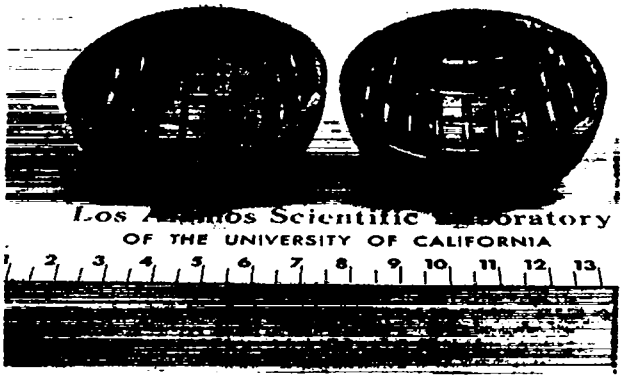

Fig. 2.
Hemishells of D-38 used in Test 1. The hemishell on the right has U-shaped grooves; the one on the left has V-shaped grooves.

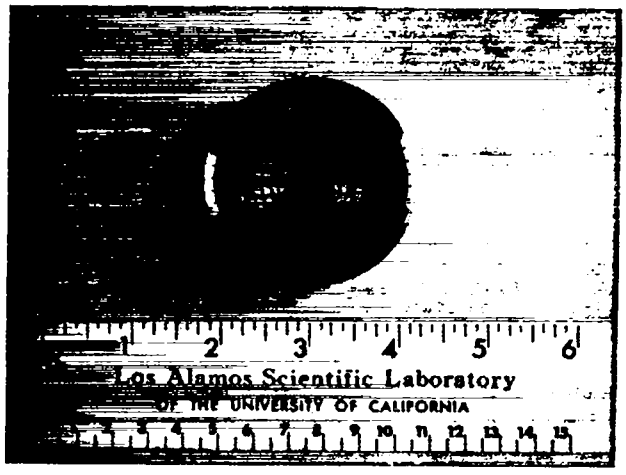

Fig. 3.
A scored hemishell of tungsten used in Test 5. A similar hemishell of tungsten alloy completed the assembly.

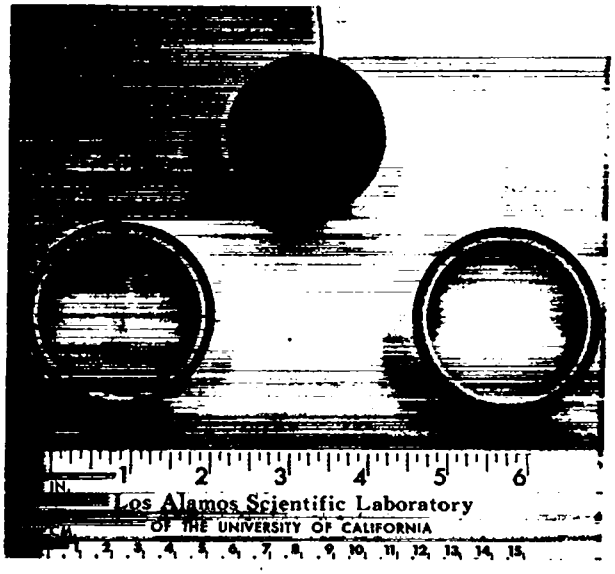

Fig. 4.
Scored tungsten hemishells fitted with RTV silicone-rubber liners and a spherical charge of PBX-9404.

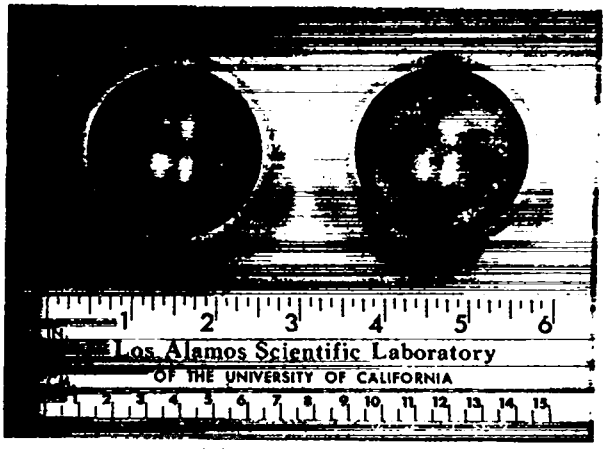

Fig. 5.
Lead and copper hemishells containing a dispersion of 3.2-mm-diam tungsten-alloy spheroids. The lead hemishell is on the right.

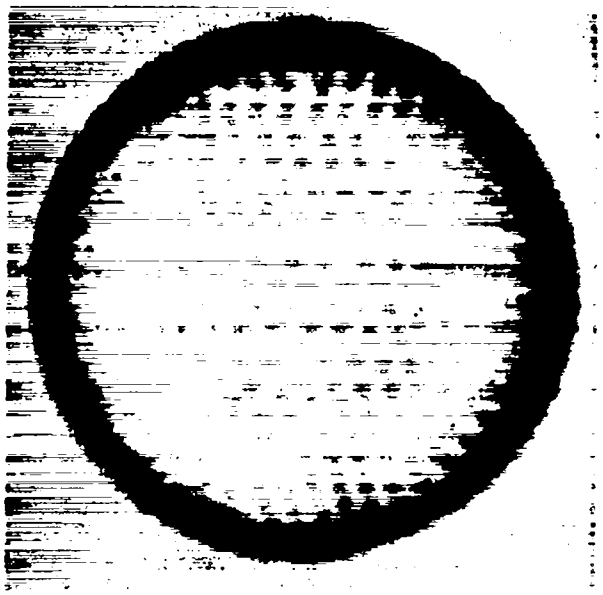

Fig. 6.
A typical radiograph of a lead hemishell used in Tests 3 and 6 showing the arrangement of the 500 tungsten-alloy spheroids.

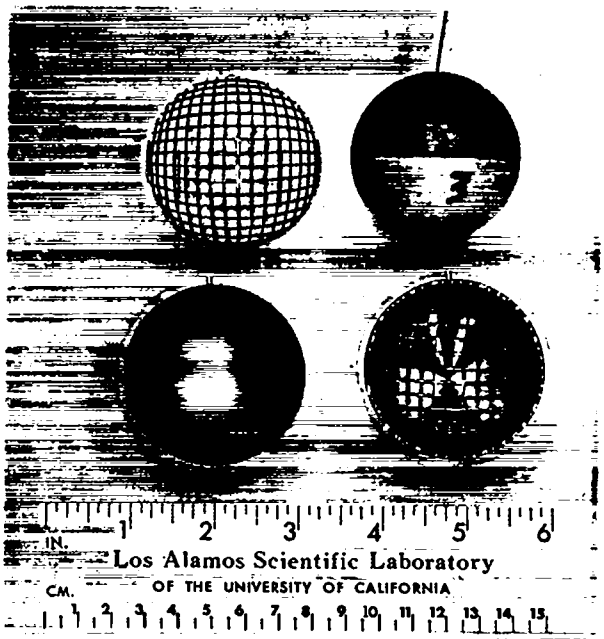

Fig. 7.
Tungsten and tungsten-alloy hemishells with copper-screen fragmetation initiators and a spherical charge of PBX-9404. (The PBX-9404 is labeled 3.)

Fig. 8.
Close-up of test arena with the device suspended in center of photograph.

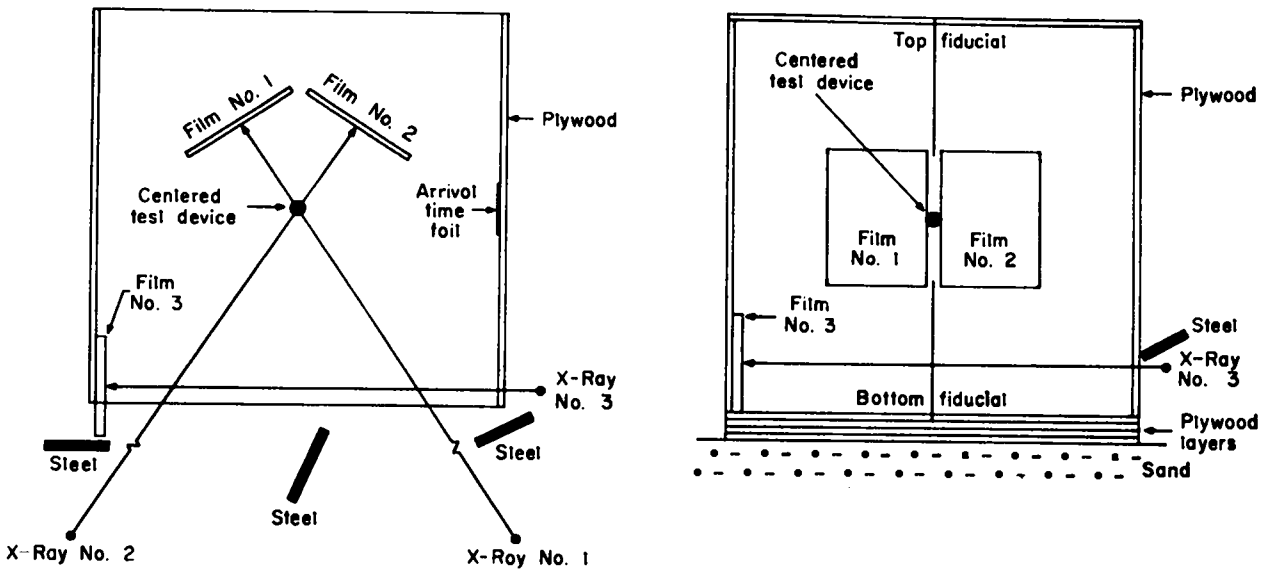

a. Top view. *b. Front view.*

Fig. 9.
Experimental arrangement.

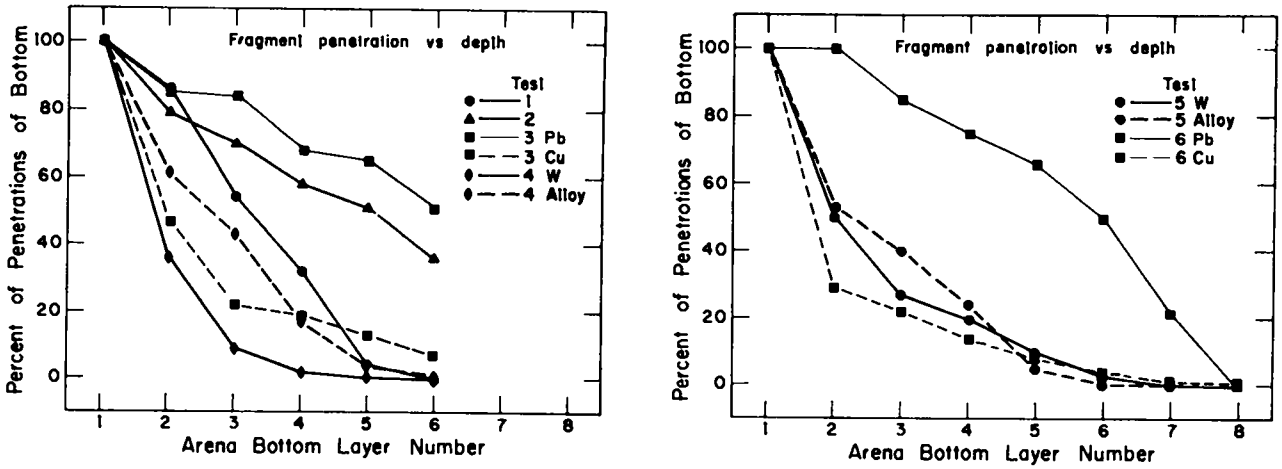

a. Tests 1-4. *b. Tests 5 and 6.*

Fig. 10.
Relative penetration of fragments.

a. At 37.64 μs after first significant case motion.

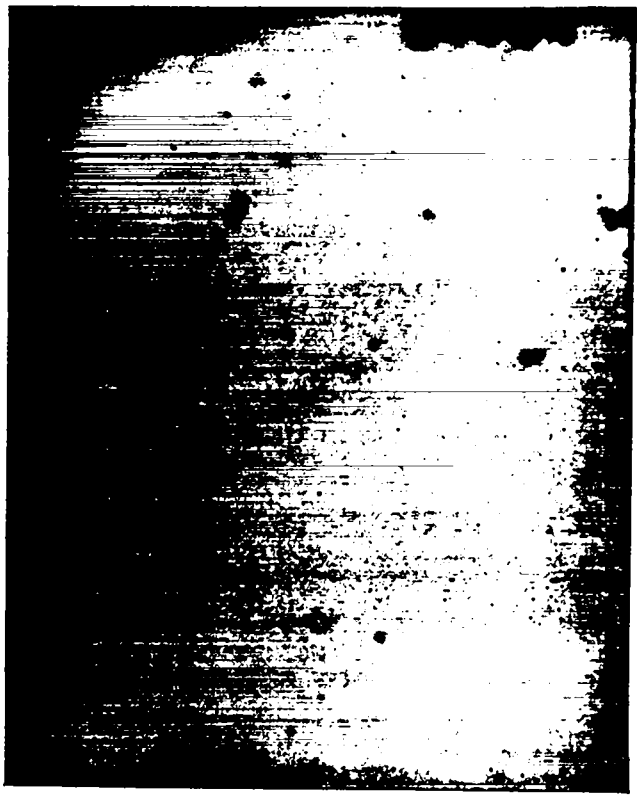

c. At 432.49 μs after first significant case motion. View taken across edge of expanding shell of fragments.

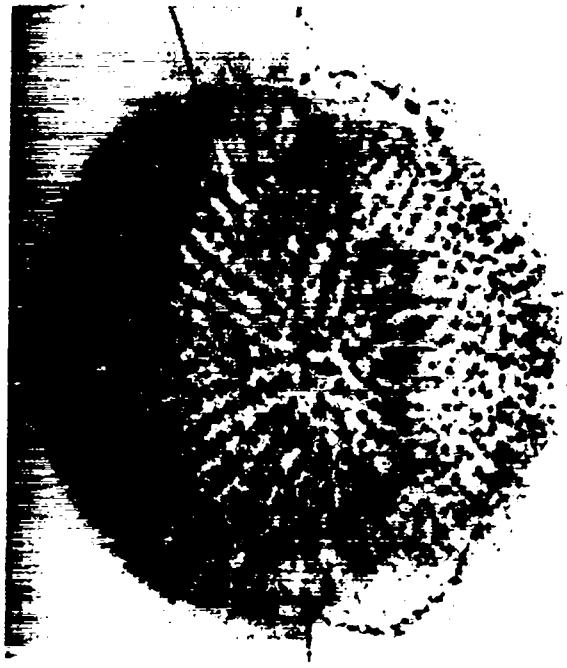

b. At 62.43 μs after first significant case motion.

Fig. 11.
Flash radiograph of case fragments from Test 6. In a and b the lead-matrix hemisphere is to the left in the photograph; copper is to the right.

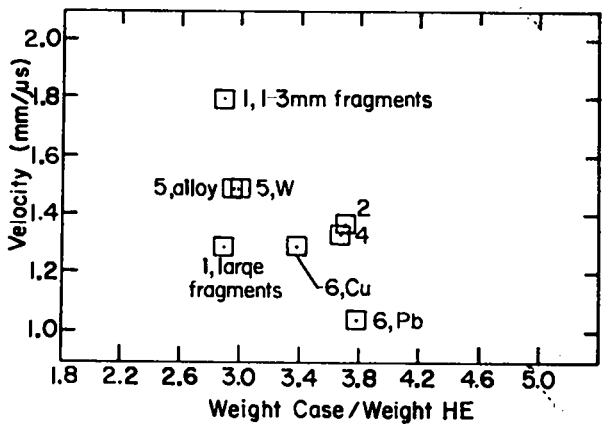

Fig. 12.
Plot of weight ratio vs fragment velocity.

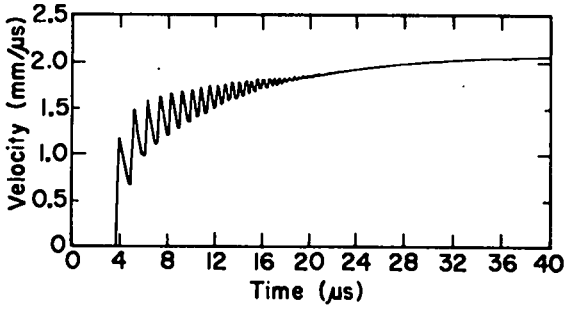

Fig. 13.
Calculated velocity for problem T-178.

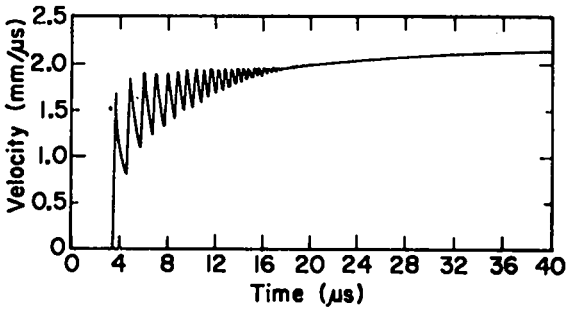

Fig. 15.
Calculated velocities for problem T-179.

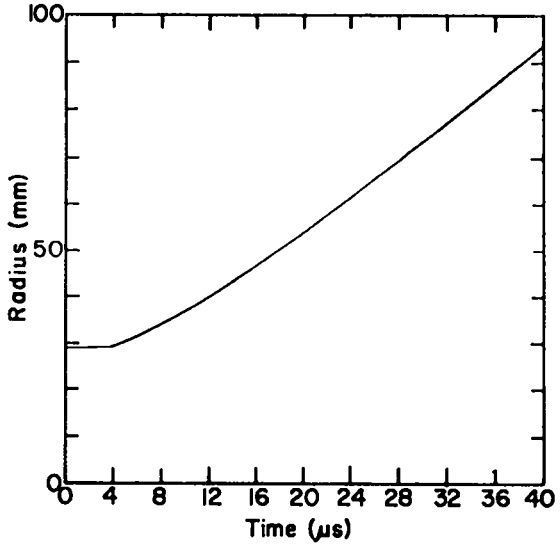

Fig. 14.
Calculated radii for problem T-178.

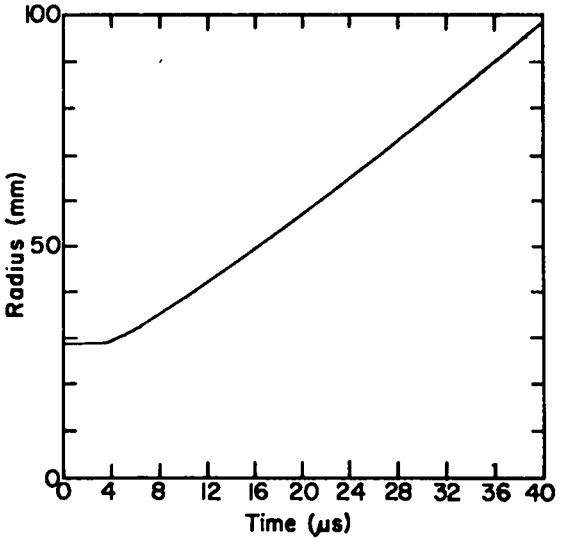

Fig. 16.
Calculated radii for problem T-179.

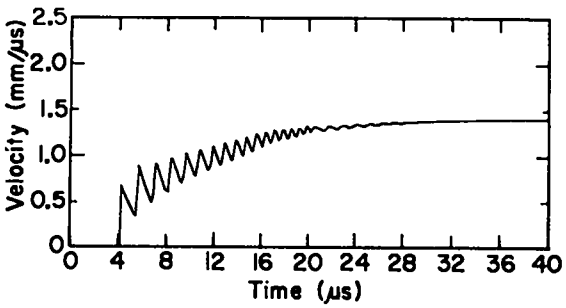

Fig. 17.
Calculated velocities for problem T-180.

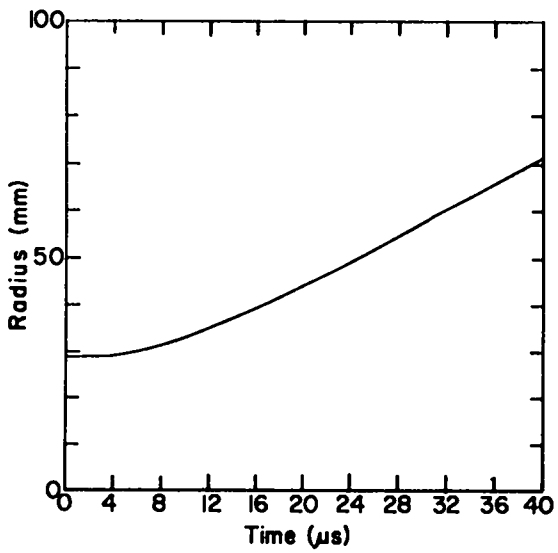

Fig. 18.
Calculated radii for problem T-180.

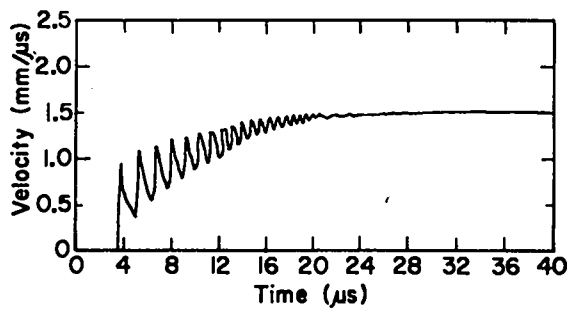

Fig. 19.
Calculated velocities for problem T-181.

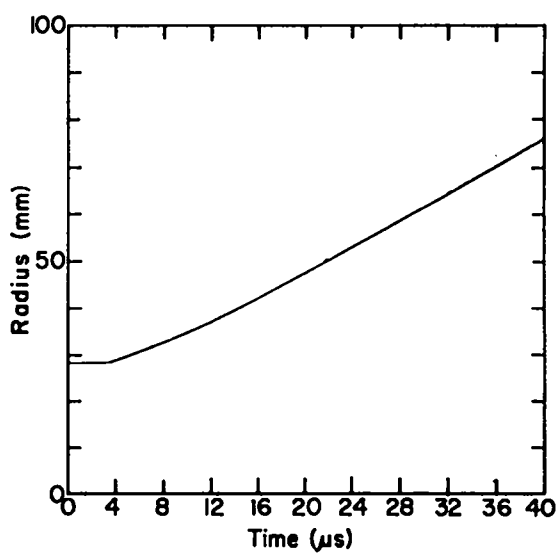

Fig. 20.
Calculated radii for problem T-181.

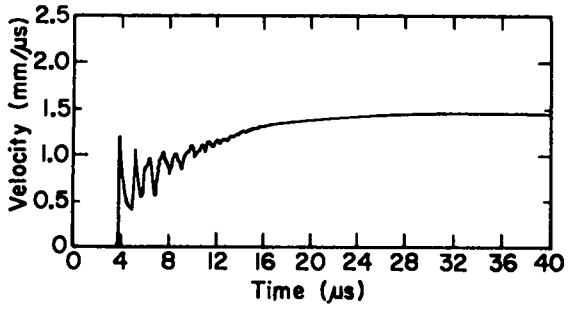

Fig. 21.
Calculated velocities for problem T-182.

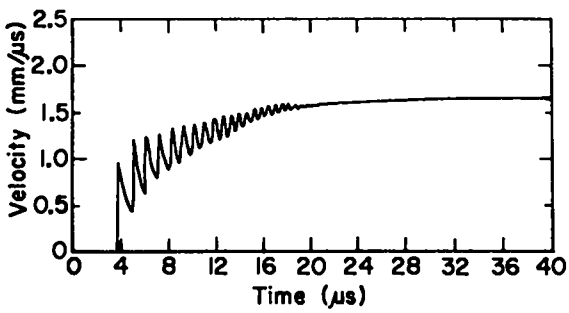

Fig. 23.
Calculated velocities for problem T-184.

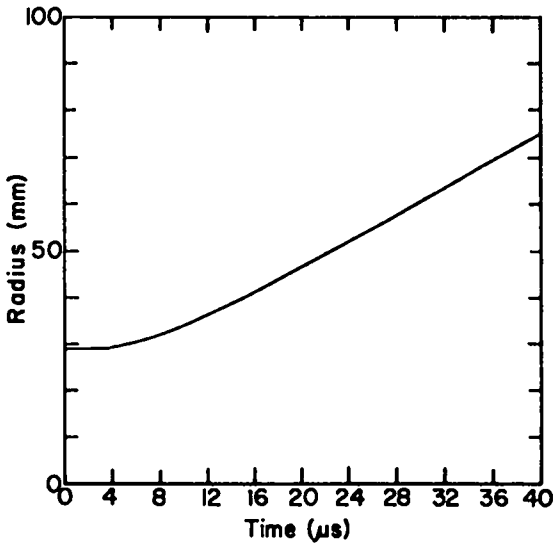

Fig. 22.
Calculated radii for problem T-182.

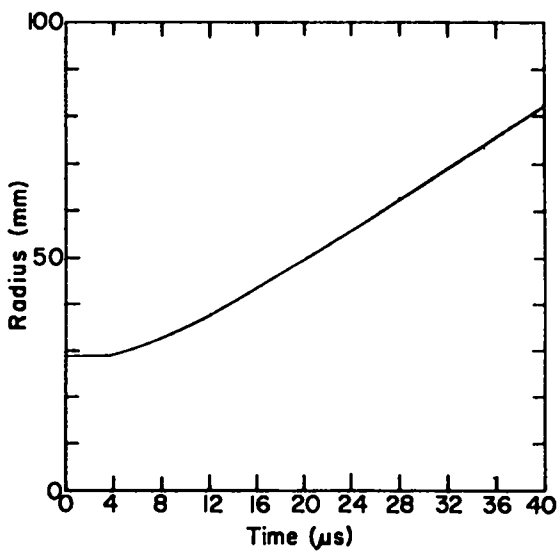

Fig. 24.
Calculated radii for problem T-184.

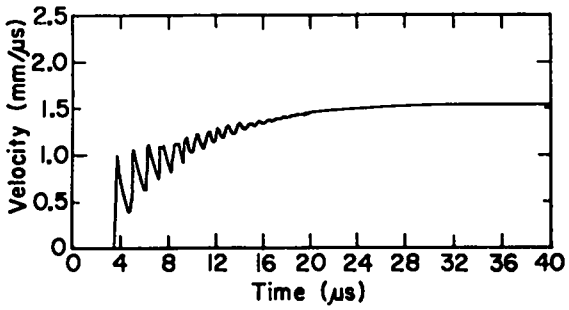

Fig. 25.
Calculated velocities for problem T-185.

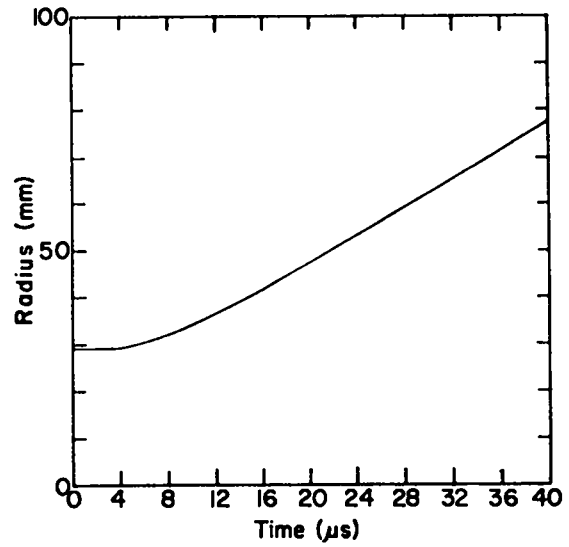

Fig. 26.
Calculated radii for problem T-185.

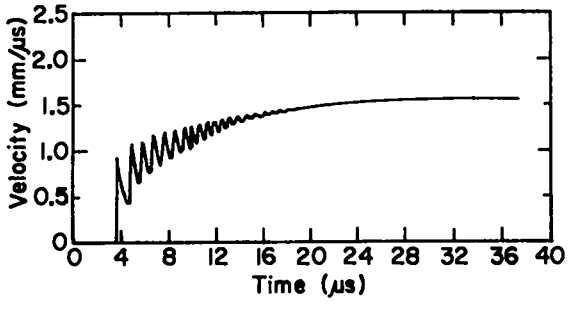

Fig. 27.
Calculated velocities for problem T-186.

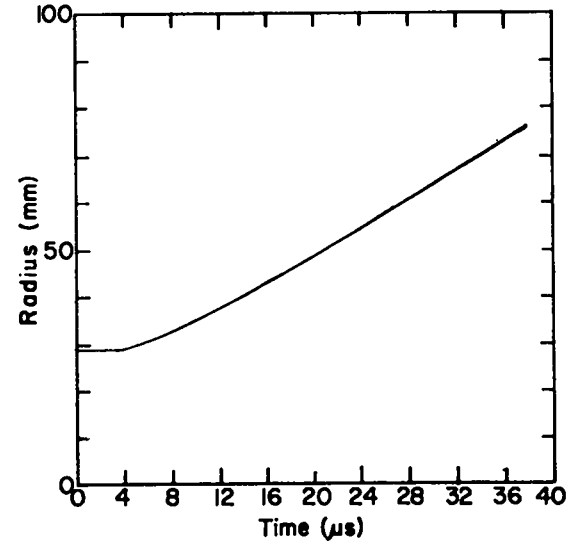

Fig. 28.
Calculated radii for problem T-186.

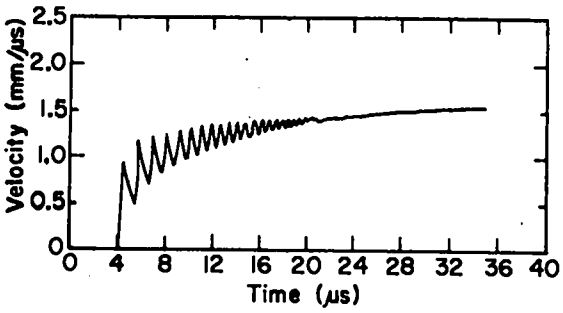

Fig. 29.
Calculated velocities for problem T-188.

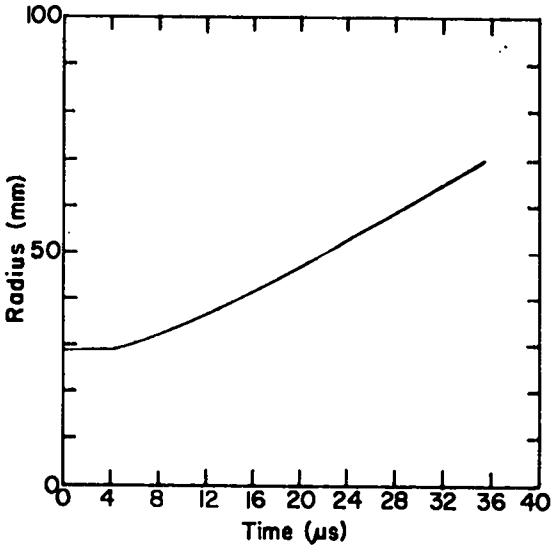

Fig. 30.
Calculated radii for problem T-188.

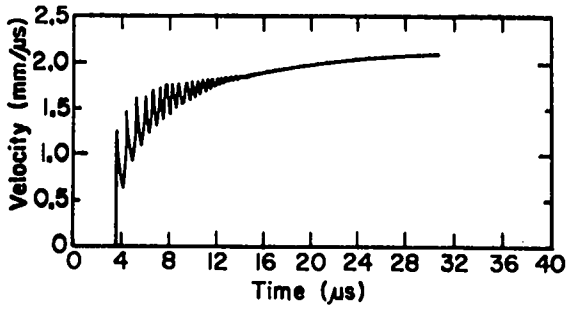

Fig. 31.
Calculated velocities for problem T-190.

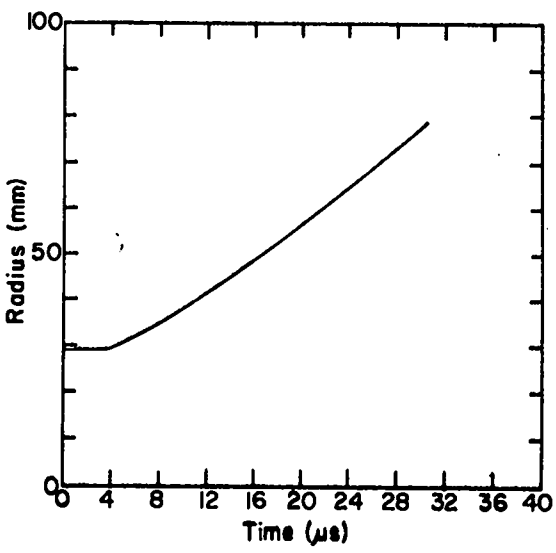

Fig. 32.
Calculated radii for problem T-190.

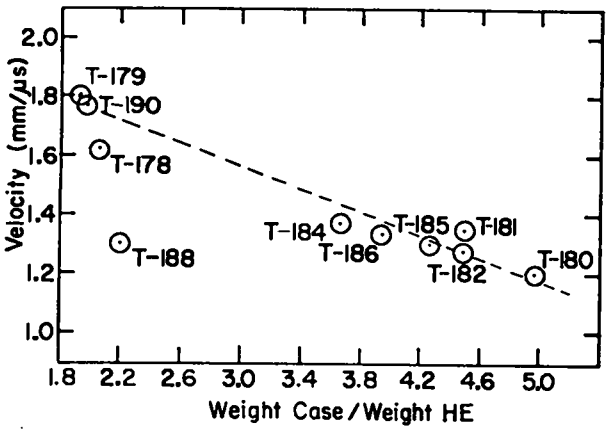

Fig. 33.
Calculated velocity vs case weight/HE weight.

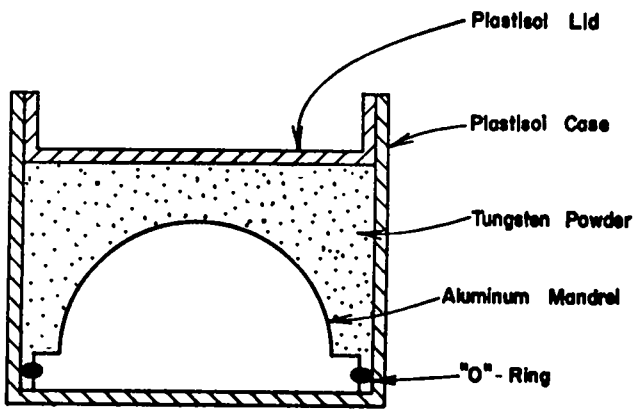

Fig. 34.
Isostatic pressing arrangement.

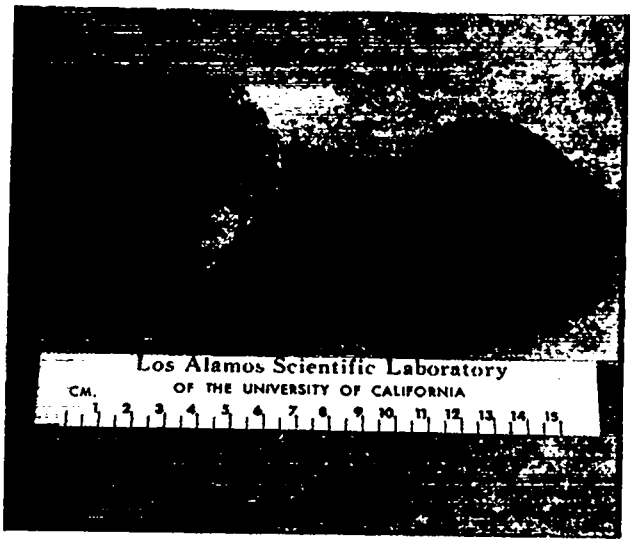

Fig. 35.
The specimen on the left is a tungsten preform, on the right, a completed tungsten case.

Fig. 36.
Typical microstructure of tungsten case used in Test 4. The case was sintered from 0.64-μm powder for 4 h at 1975 K in hydrogen.

Fig. 37.
Typical microstructure of the tungsten case used in Test 5, showing the effect of vacuum sintering the material from Fig. 35 for 2 h at 2475 K.

Fig. 38.
Typical microstructure of a liquid-phase-sintered alloy of W-3.5 Ni-1.5 Fe. The microstruture is similar to that of the alloy cases used in Tests 4 and 5. The tungsten-rich phase is the spherical-shaped grains.

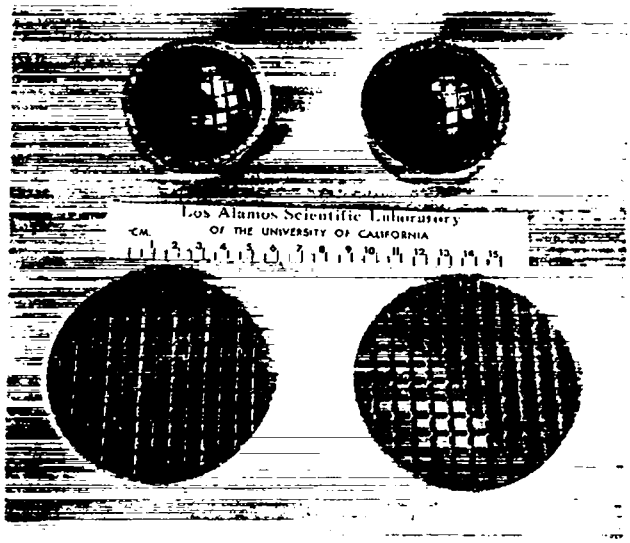

Fig. 39.
Starting blanks and cupped specimens of D-38: the specimens on the right have a U-shaped groove pattern; those on the left are V-shaped.

Fig. 40.
Microstructure of the tungsten-alloy spheroids.

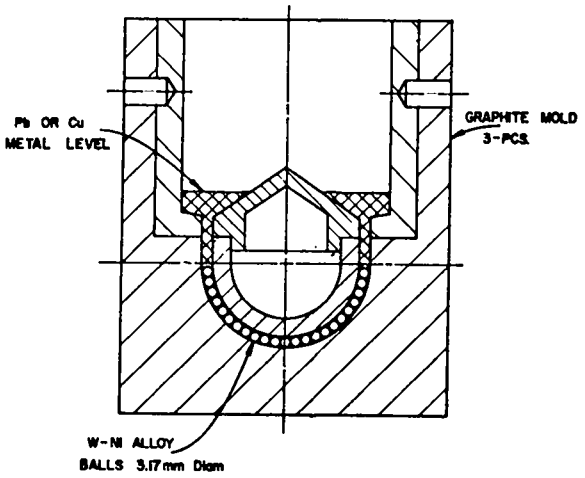

Fig. 41.
Graphite mold assembly for casting composite cases of either lead or copper with tungsten-alloy spheroids.

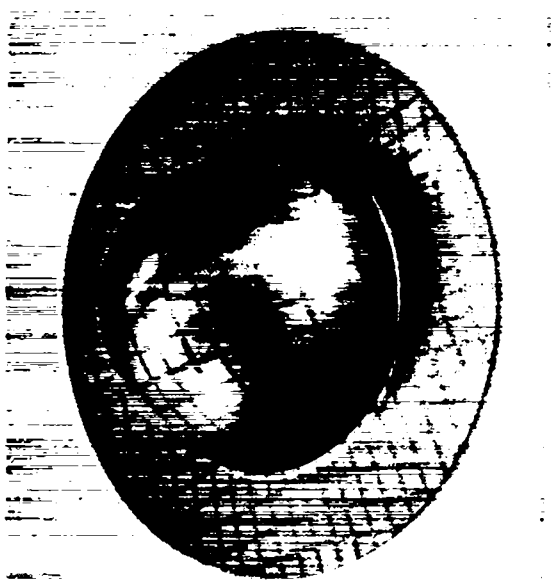

Fig. 42.
A cupped and partially etched copper blank ready for etching into a screen hemisphere.

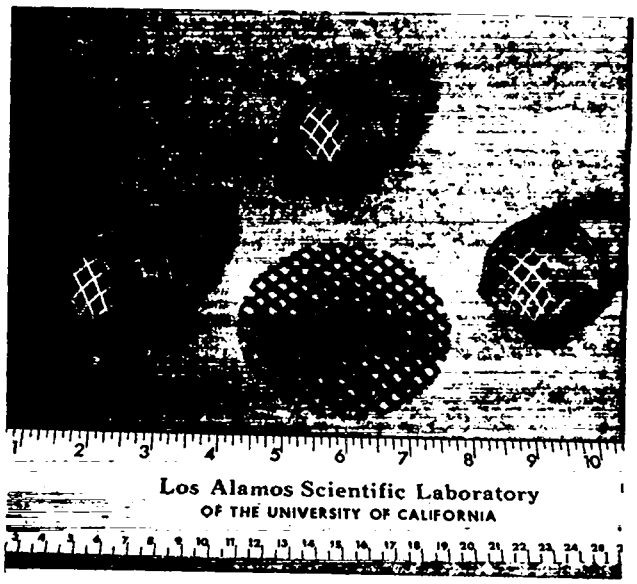

Fig. 43.
Hemispheres formed by deep drawing steel blanks similar to the one shown.